Journal of the Serbian Society for Computational Mechanics / Vol. 19 / No. 1, 2025 / pp 245-265 / review paper
(10.24874/jsscm.2025.19.01.15)

STRONG COUPLING IN MODELING SOLID-FLUID INTERACTION IN PAK SOFTWARE - THEORY AND SELECTED APPLICATIONS

Velibor Isailovic[1,*] [0000-0002-1417-9633], Miljan Milosevic[2.3] [0000-0003-3789-2404], Nikola Kojic[4] , Milos Kojic[5.6] [0000-0003-2199-5847]

[1]Faculty of Engineering, University of Kragujevac, Sestre Janjic 6, 34000 Kragujevac, Serbia
[2]Institute of Information Technologies, University of Kragujevac, Department of Technical-Technological Sciences, Jovana Cvijica bb, 34000 Kragujevac, Serbia.
[3]Faculty of Information Technology, Metropolitan University, Belgrade, Serbia
[4]Department of Surgery and Center for Engineering in Medicine, Massachusetts General Hospital, Harvard Medical School, and Shriners Hospitals for Children, Boston, MA, USA.
[5]Bioengineering Research and Development Center BioIRC Kragujevac, Prvoslava Stojanovica 6, 3400 Kragujevac, Serbia.
[6]Serbian Academy of Sciences and Arts, Knez Mihailova 35, 11000 Belgrade, Serbia
*corresponding author

Abstract

Finite element (FE) modeling the motion of deformable bodies within a fluid, as well as the interaction between the bodies, has been a continuous challenge over the years. There are in principle two approaches – loose and strong coupling between the FE models of the two domains, with their advantages and drawbacks. We here present our concept of strong coupling which we thoroughly tested in the past, particularly with respect to the accuracy of the model, Theoretical background and computational procedure are briefly described and then illustrated on two typical applications, among numerous in our references. One is related to the microfluidic chip and another – to conditions of the passing of the circulating tumor cells (CTCs) through a capillary narrowing; both are significant in biomedical engineering. Regarding the first example, we have that in recent years, attention has been paid to the creation of the so-called microfluidic chips. These devices are used for testing very small blood samples. There, blood is passed through a micro-device in which cells are separated according to cell stiffness under precisely controlled laminar flow conditions. The development of the microfluidic chip can be significantly accelerated and simplified by building its computational replica - a computer program designed for modeling the chip's geometry and topology, as well as simulating the processes occurring within it. In the second example, we explored the parameter space, where a relationship between the capillary blood pressure gradient and the circulating tumor cells (CTCs) mechanical properties (size and stiffness) was determined for the CTC arrest in a capillary. The presented computational platform, along with the derived pressure–size–stiffness relationship, serves as a valuable tool for investigating the biomechanical conditions underlying capillary arrest of circulating tumor cells (CTCs) and CTC clusters, enabling predictive modeling of metastatic progression based on biophysical CTC parameters, and supporting the rational design of size-based CTC isolation technologies that account for large CTC deformations under high pressure gradients.

Keywords: Solid-fluid interaction, strong coupling, microfluidic chip, circulating tumor cells, cell arrest, metastasis

1. Introduction

Computer modeling is developed to represent the behavior of physical objects. These objects span from a simple component like a tooth of the gear to a complex system like an automatic transmission gearbox or whole vehicle. Also, computer simulations can be applied in various fields of science and technology.

The first topic of this paper is the application of computer algorithms and methods to develop a computational model (Aceto et al. 2014; Isailovic et al. 2014) of a microfluidic chip (Fabienne et al. 2022). The microfluidic chip is a device that allows the control and manipulation of tiny volumes of fluids, often on the order of nanoliters or picoliters. These chips contain a mesh of microchannels, chambers, and valves that can be used for a variety of applications, including biological assays, chemical reactions, and diagnostics.

A computational model of a microfluidic chip simulates its physical behavior, including analysis of fluid and solid dynamics, fluid-solid interaction, solid-solid interaction, and other processes within the design (Kojic et al. 2015).

Microfluidic chips for blood cell separation represent a sophisticated application of microfluidics to isolate specific types of blood cells from blood samples or even whole blood. This technology has significant implications for medical diagnostics, therapeutic monitoring, and research. Microfluidic chips leverage the principles of fluid dynamics at the microscale to separate blood cells based on their physical and/or biochemical properties. One of the popular techniques is the so-called size-based separation (Hao et al. 2018). Channels and filters within this type of microfluidic chip are designed to allow cells with specific sizes and elasticity to pass through while blocking or redirecting others. For example, red blood cells (RBC) can be separated from white blood cells (WBC) based on size differences. Also, tumor cells can be separated from RBCs or WBCs.

Topology optimization of the microfluidic chip plays an important role in the development and enhancement phase. To ensure successful cell separation, it is essential to adjust the chip topology in terms of shape and dimensions. This way of development, which can be characterized as a trial-and-error method, can be significantly accelerated and improved by developing a specialized computer simulation: a software tool that would trustworthily simulate the process inside the chip and enable the quick execution of tens or hundreds in-silico experiments (also trial-and-error, but much faster and cheaper) with the aim of finding the optimal topology.

Such a software implementation requires coupling of fluid dynamics (for the fluid part of blood), solid dynamics (for blood cells and the microfluidic chip), the fluid-solid interaction (between the fluid part of blood and blood cells, but also between blood and the chip), as well as the solid-solid interaction (between cells or between a cell and the chip).

In the second topic, we briefly summarize the basic physiological conditions for motion and arrest of the Circulating Tumor Cells (CTCs) in capillaries. Circulating tumor cells (CTCs) indicate the initiation of cancer metastasis, according to,e.g., Lianidou et al. 2011, Maheswaran et al. 2010. Various technologies (Pantel et al. 2008) (e.g. microfluidic devices Karabacak et al. 2014; Ozkumur et al. 2013) have been employed to isolate CTCs from blood samples. It was found that the CTC clusters in the circulation are important in metastasis (Aceto et al. 2014; Cho et al. 2012, Stott et al. 2010; Yu et al. 2013). CTCs or larger CTC clusters in general need

to traverse through capillary beds, where the diameter of a capillary is around 7 microns (Berne et al. 2010; Maton 1993), while the CTCs can be as large as ~20μm, and the CTC clusters can be on the order of 100μm (Karabacak et al. 2014; Ozkumur et al. 2013; Stott et al. 2010). Therefore, CTCs can be prevented from passing through capillaries (Weinberg 2013; (Shibue et al. 2011). The arrest of CTCs in capillaries can be a key part of the metastatic process (Shibue et al. 2011; Balzer et al. 2012). Additionally, the onset of leukostasis, where cancer cells aggregate within the vasculature can cause grave clinical symptoms (Lam et al. 2011; Lichtman 1973; Rosenbluth et al. 2006). Two mechanisms can be distinguished: 1) the interaction of the cells with the vasculature, and 2) the size and mechanical properties of the cells coupled to the local fluid conditions. There has been considerable focus on the mechanism (1) (Shibue et al. 2011; Balzer et al. 2012), while the effect of the (2) is not well understood.

This paper presents a custom computational platform developed to simulate the deformation and transport of large viscoelastic solids (CTCs) through microvascular constrictions. The model focuses on the passage of large-diameter CTCs through capillaries with characteristic diameters of approximately 7 μm, identifying the key biophysical parameters governing this process.

Simulation results reveal a direct relationship among three critical factors: (1) CTC diameter, (2) CTC stiffness, and (3) the fluid pressure gradient across the capillary. By exploring a wide range of values for diameter and stiffness, the model provides predictive insights into the arrest or transit of CTCs under physiological conditions. The pressure–size–stiffness relationship indicates that, for a given pressure gradient, cell stiffness significantly limits the maximum cell diameter capable of successful entry. Specifically, even very large cells (~100 μm) can traverse capillaries if sufficiently soft (~10 Pa), whereas stiffer cells (~1000 Pa) are predicted to arrest when their diameter exceeds ~12 μm.

These findings provide understanding of CTC dynamics in confined environments and have direct implications for metastasis modeling and the design of size-based CTC isolation technologies, where large deformations under physiological pressure gradients have to be considered (Zhang et al. 2014).

From a modeling point of view, the motion of a deformable body is described using Newton's equation of motion (Kojic et al. 2008), and the flow of a viscous incompressible fluid is described using Stokes' or Navier-Stokes equations (Kojic et al. 2008). The solid equations are derived in the Lagrangian formulation (Kojic et al. 2008). On the other hand, fluid flow equations are derived using Euler's formulation supported by the definition of material derivative, where the field of physical quantity is defined by fixed geometric points of space and material points pass through it.

These equations can be applied in integral form over the fluid and solid domains. Afterwards, a discrete system of equations is obtained by applying the finite element method. The solution vectors of these systems give the nodal values: velocity and pressure for the fluid domain and displacement (or velocity) for the solid domain.

However, there are missing pieces: the application programming interface between existing in-house developed CFD and CSD solvers (Kojic et al. 2017) that is able to couple the fluid domain and the solid domain at their boundary interface, and an additional CSD module dedicated to solid-solid interaction (Figure 1). The focus of this paper is the development of software that will connect independently developed solvers and enable the implementation of specific boundary conditions imposed by complex solid-fluid and solid-solid interaction problems.

Figure 1: The architecture of the software solution: Relations and missing pieces (bold)

A special challenge here is the variety of programming languages used in the implementation of individual building blocks: FORTRAN77 (for existing FEM solvers from PAK (Kojic et al. 2017)) FORTRAN95 (for APIs) C and C++ for assembling sparse matrices - the inputs to the powerful sparse solver MUMPS (Amestoy et al. 1999), which is parallelized based on the MPI library to achieve quick running of computationally demanding simulations.

2. Theoretical background and computational procedure

2.1 The basic equations

This section summarizes the governing equations and the remeshing procedure employed in the analysis. The Navier–Stokes equations, which describe the conservation of linear momentum, are used to model the fluid domain. For a Newtonian fluid, these equations take the following form: (Kojic et al. 2008):

$$\rho_f \left(\frac{\partial v_i}{\partial t} + v_j \frac{\partial v_i}{\partial x_j} \right) = -\frac{\partial p}{\partial x_i} + \mu \frac{\partial^2 v_i}{\partial x_j^2} + f_i^B,\ i = 1,2,3; sum\ on\ k: k = 1,2,3 \tag{1}$$

where v_i are fluid velocities, p is pressure, f_i^B are volumetric forces; and ρ_f and μ are fluid density and dynamic viscosity. By neglecting the inertial terms on the left-hand side, the Navier–Stokes equations reduce to the well-known Stokes equations, which describe slow, viscous-dominated flows:

$$-\frac{\partial p}{\partial x_i} + \mu \frac{\partial^2 v_i}{\partial x_j^2} + f_i^B = 0,\ i = 1,2,3; sum\ on\ k: k = 1,2,3 \tag{2}$$

In addition to the momentum equations, the continuity equation for an incompressible fluid has to be satisfied:

$$\frac{\partial \rho}{\partial t} + v_i \left(\frac{\partial \rho}{\partial x_i} \right) = 0 \tag{3}$$

The governing equations can be transformed into a weak form using a weighted residual procedure, as described in [Kojic et al., 2008]. For the Navier–Stokes model, the incremental-iterative matrix form of the balance equations at time step n, with a step size Δt, including the continuity condition (3), can be expressed as follows:

$$\begin{bmatrix} \frac{1}{\Delta t}\mathbf{M} + {}^{n+1}\hat{\mathbf{K}}_{vv}^{i-1} & \mathbf{K}_{vp} \\ \mathbf{K}_{vp}^{T} & \mathbf{0} \end{bmatrix} \begin{Bmatrix} \Delta \mathbf{V}^{i} \\ \Delta \mathbf{P}^{i} \end{Bmatrix} = \begin{Bmatrix} {}^{n+1}\mathbf{F}_{ext}^{i-1} \\ \mathbf{0} \end{Bmatrix} - \begin{bmatrix} \frac{1}{\Delta t}\mathbf{M} + {}^{n+1}\mathbf{K}_{vv}^{i-1} & \mathbf{K}_{vp} \\ \mathbf{K}_{vp}^{T} & \mathbf{0} \end{bmatrix} \begin{Bmatrix} {}^{n+1}\mathbf{V}^{i-1} \\ {}^{n+1}\mathbf{P}^{i-1} \end{Bmatrix} + \begin{Bmatrix} \frac{1}{\Delta t}\mathbf{M}\,{}^{n}\mathbf{V} \\ \mathbf{0} \end{Bmatrix} \tag{4}$$

where matrix $\mathbf{M}$ corresponds to the local velocity derivatives $\frac{\partial v_i}{\partial t}$; matrices $\hat{\mathbf{K}}_{vv}^{i-1}$ and $\mathbf{K}_{vv}^{i-1}$ include convective velocity derivatives $\frac{\partial v_i}{\partial x_k} v_k$ and viscous terms; $\mathbf{K}_{vp}$ is the matrix coupling velocities and pressure; $\mathbf{F}_{ext}$ are external nodal forces corresponding to volumetric forces and action of the surrounding elements; $\mathbf{V}$ and $\mathbf{p}$ are nodal velocity and pressure vectors ($\boldsymbol{V}^n$ is velocity at start of time step); and the right upper indices i and $i-1$ denote the current and previous equilibrium iteration within time step. An implicit time integration scheme is employed, whereby the system of balance equations is enforced at the end of each time step. Iterations are performed until predefined convergence criteria are met. Further details regarding the matrix formulation and computational procedures can be found in (Kojic et al., 2008).

Moving particles are modeled using individual meshes assigned to each particle. The balance equations for a solid finite element are derived from Newton's second law and can be expressed in the following form:

$$\left(\frac{\mathbf{M}}{\Delta t} + {}^{t+\Delta t}\mathbf{K}^{(i-1)}\,\Delta t\right)\Delta \dot{\mathbf{U}}^{(i)} = {}^{t+\Delta t}\mathbf{F}_{ext} - \mathbf{F}_{int}^{(i-1)} - \frac{\mathbf{M}}{\Delta t}\left({}^{t+\Delta t}\dot{\mathbf{U}}^{(i-1)} - {}^{t}\dot{\mathbf{U}}\right) \tag{5}$$

Where $\mathbf{M}$ and $\mathbf{K}$ are the mass and stiffness matrix of the solid, $\dot{\mathbf{U}}$ is the nodal velocity vector; $\mathbf{F}_{ext}$ are external nodal forces which include volumetric forces, and nodal forces from other elements - together with forces from fluid elements for nodes on solid – fluid boundary interface; and $\mathbf{F}_{\text{int}}$ are internal nodal forces arising from stresses within solid (total Lagrangian formulation is used here) (Kojic et al. 2008). Note that the term ${}^{t+\Delta t}\mathbf{K}^{(i-1)}\,\Delta t$ is used for better convergence (it does not affect the solution which only depends on the right-hand side of equation (5)).

2.2 The basic concept description

In the Introduction section, the building blocks of the software solution, that will simulate the flow through a microfluidic chip, are mentioned (finite element solvers for computational solid and fluid dynamics (Kojic et al. 2017)). However, those building blocks alone are not enough. They are independent entities that enable the simulation of different physical fields, without the possibility of their mutual interaction.

In order to establish interconnection and interaction between these blocks, it is necessary to develop application programming interface between CFD and CSD solvers (FSI API), and additional Solid - Solid Interaction Module (SSI Module). The role of the FSI API is to enable

interconnection on the fluid – solid boundary. The role of the SSI Module is to enable interaction between two different solid domains, e.g. between two blood cells or between a cell and chip.

The basic idea of this concept is the discretization of the entire fluid and solid domain with a continuous finite elements mesh. The problem of fluid-solid interaction assumes the moving of solid bodies in the fluid. In order to reproduce this phenomenon in software, finite element mesh has to be modified over time, according to the motion of solid bodies. The scale of solid deformations does not require remeshing of the solid mesh. However, moving the solid bodies requires changing the boundaries of the fluid, i.e. the fluid mesh has to be modified and updated at the end of each time step.

The methodology based on remeshing assumes equal velocity at geometrically matched fluid and solid boundary nodes. That means the degree of freedom (or equation) corresponding to the velocity of the solid boundary node is at the same time the degree of freedom of the fluid velocity at the corresponding fluid boundary node. Furthermore, it implies that each boundary node's degree of freedom has only one equation, regardless of belonging to both domains. Those equations have contributions from both domains, i.e. individual equations from the fluid and the solid were combined by addition into a single equation.

When the system of equations is solved for a single time step, the position of the solid is updated based on the solution for the solid velocities.

$$ {}^{t}\beta \overset{\substack{u(t)\\ v(t)}}{\Rightarrow} {}^{t+\Delta t}\beta \tag{6} $$

As already described, the concept of solving the fluid flow equations assumes stationary finite element mesh. For the new position of the solid, there is no longer a coincidence of the solid and fluid boundary nodes. Therefore, a new mesh has to be created with interpolated velocities and pressures from the old mesh.

The previous paragraphs describe the problem that the FSI API solves. Conceptually, it looks like in Figure 2. Figure 2a shows the solid and the fluid mesh separately, and Figure 2.b shows the mesh in the case when the solid and fluid are coupled. In the following, the mesh update procedure and the "mapping" (projection) of velocities and pressures in the new mesh based on the last known solution will be explained in detail.

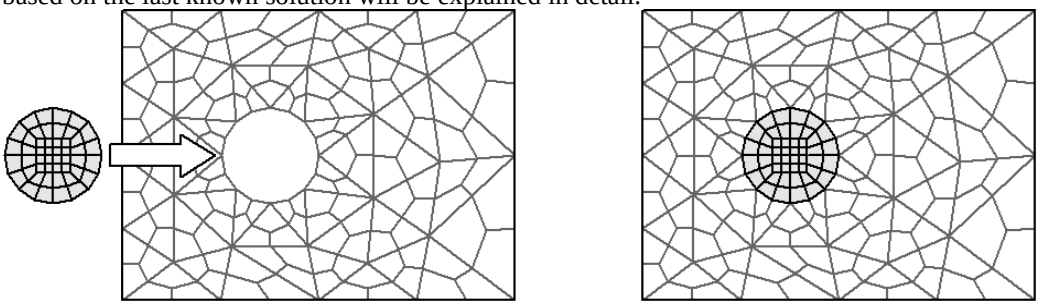

Figure 2: Solid and fluid finite element mesh

2.3 The FSI API: Coupling of solid and fluid equations into a single system

The system of equations that needs to be solved consists of equations that describe fluid and solid dynamics. Connection of these equations is achieved in geometrically coincided nodes at the fluid-solid boundary (Figure 3).

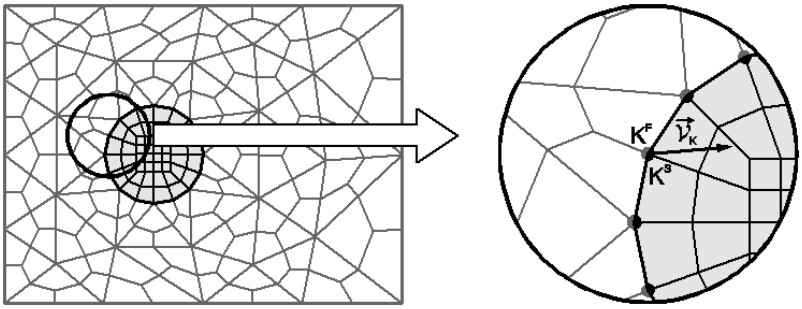

Figure 3: Merged mesh with matched fluid and solid nodes

Hence, in the system of equations first are assembled fluid equations and then solid equations. Both subsystems of equations have their numeration (IDs). But, for the solid nodes located on the fluid-solid boundary, the equation IDs are taken from the fluid subsystem. Therefore, the solid contour nodes and the corresponding fluid nodes have the same equation IDs, i.e. the same degrees of freedom:

$$v_{Ki}^{f} = v_{Ki}^{s}, \quad i = 1,3 \tag{7}$$

where the index i indicates the velocity components in the Cartesian coordinate system, and the index K indicates the current node on the boundary.

Solid mesh is built once, and most often it is performed using regular (structural) finite element meshes. During building, nodes located on the outer boundary of the solid and their order are identified (in an arbitrary direction). These nodes represent the boundary towards the fluid domain (fluid mesh).

Fluid mesh is generated at each time step. Since the solid domain position, shape, and number of subdomains (different solid bodies) can be arbitrary, unstructured finite element mesh is a better choice. One of the most often used unstructured mesh building algorithms is the so-called Delaunay triangulation (Ito 2015). The triangle as a finite element is widely used, but for the problem of solving the Navier-Stokes equations, an optimal solution in terms of the accuracy of the results is four-node finite element mesh. Therefore, the program Triangle (Shewchuk) is applied, and the triangles obtained as an output from this program are divided into three four-node finite elements using the TriangleToQuadConverter (Milasinovic et al. 2020).

At the initial time step, the known values are positions of the solid nodes and IDs of solid contour nodes. In the fluid domain, the geometry of the walls and information about the given boundary conditions on that contour are known. The structure of the main program is given in Figure 4. The program contains solvers for solving coupled systems of equations. The connection between solvers is achieved by the FSI API. Based on data about solid and fluid domains, the Mesh Generator (program based on Triangle) and Mesh Converter (program based on TriangleToQuadConverter0) build a mesh with appropriate boundary conditions. Those data are used by CFD and CSD solvers.

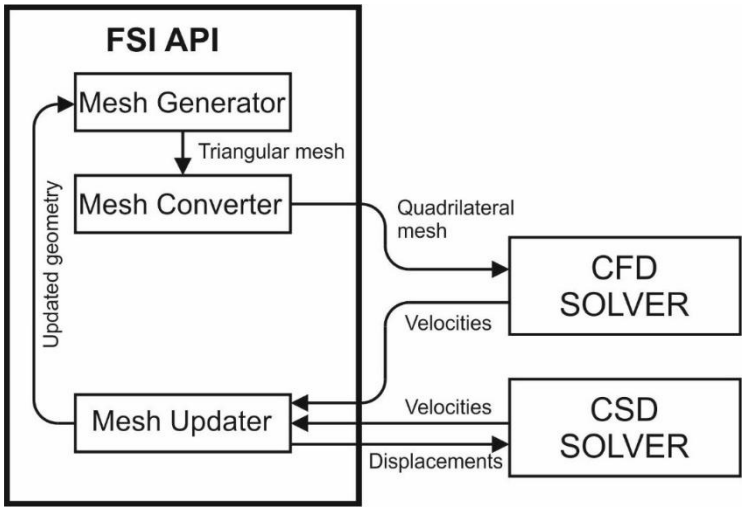

Figure 4: Structure of the main program

At the end of each time step, when convergence was achieved, a solution for the solid velocity, fluid velocity and pressure was obtained. Based on the obtained velocities, the displacements of the solid can be calculated:

$$^{t+\Delta t}\mathbf{u}_k = ^{t+\Delta t}\mathbf{v}_k \Delta t, \quad k = 1, N \tag{8}$$

where is:

N - the total number of solid nodes,

Δt - the size of the integration time step.

Given the fact Imam jedan komentar, ali ni sam ne znam kako realizovati. Univerzitet je i do sada izdavao nekakva saopstenja, koja su se ticala aktuelnih tema, na kojima se i sada insistira. Dosadasnja saopstenja su bila u najmanju ruku blaga (npr. u nekom obavestenju stoji da se od nadleznih ocekuje da razmotre zahteve i na njih odgovore - a ne da se na ispunjenju zahteva insistira, recimo). Poenta ovoga sto im sada saljemo je nase ocekivanje da se nedvosmisleno stave na stranu studenata i studentskih zahteva. Jasno je i nama i njima sta se od njih ocekuje, ali to treba nekako definisati, da buduci odgovor - izgovor ne bude: nismo znali sta ste hteli. that Euler's description of the motion is used for fluid, the finite element mesh of the fluid is fixed. On the other hand, for solid dynamics, the Lagrangian description of motion is used, where a material point moves in space, and, therefore, the geometric position of the solid mesh changes over time. The concept used for modeling is based on geometrically matched boundary nodes. However, at the end of the time step, when the displacement field in the solid has been calculated and the position of the body updated, solid boundary nodes no longer match with fluid boundary nodes (Figure 5). Consequently, a new finite element mesh must be created to achieve a geometrical matching again. In general case, there is no overlap between the nodes of the old and new fluid mesh. The values of physical quantities in the new mesh need to be calculated based on the solution from the old mesh (i.e. from the previous time step).

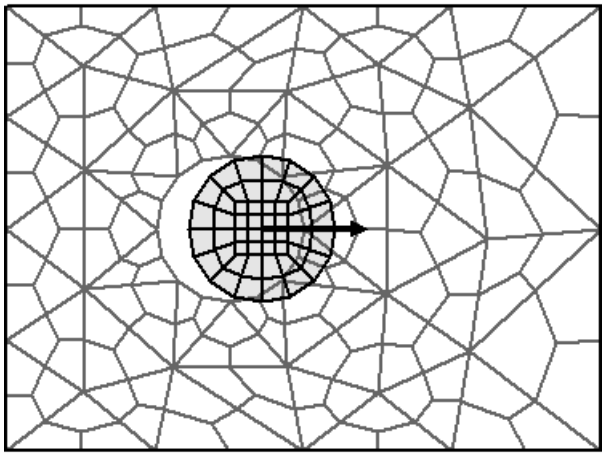

Figure 5: The position of the stationary fluid mesh and the moving solid mesh at the end of the step (no matching between fluid and solid nodes)

The mapping of velocities and pressures from the old to the new mesh is done by interpolation. For each node of the new mesh, the old mesh element it belongs to is found. Since the finite elements are polygons with four points, testing whether a node of the new fluid mesh is inside an element of the old mesh can be achieved using barycentric coordinates (Bradley 2007).

Each four-node finite element is a convex quadrilateral. Therefore, each element can be divided into two triangles made from their two connected sides and their belonging diagonal. Checking if a point (node) is inside a triangle or not is done by determining the coordinates of the point in the barycentric coordinate system of the observed triangle (Figure 6).

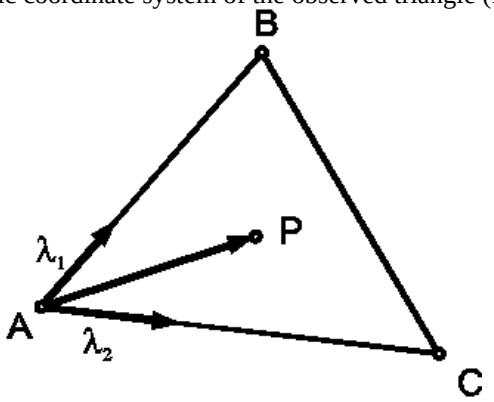

Figure 6: Barycentric coordinate system

The side vectors of the triangle are:

$$\mathbf{v}_0 = \mathbf{r}_B - \mathbf{r}_A \tag{9}$$

$$\mathbf{v}_1 = \mathbf{r}_C - \mathbf{r}_A \tag{10}$$

$$\mathbf{v}_2 = \mathbf{r}_P - \mathbf{r}_A \tag{11}$$

Barycentric coordinates are calculated as follows:

$$\lambda_1 = \frac{(v_1 \cdot v_1)(v_0 \cdot v_2) - (v_0 \cdot v_1)(v_1 \cdot v_2)}{(v_0 \cdot v_0)(v_1 \cdot v_1) - (v_0 \cdot v_1)(v_0 \cdot v_1)} \tag{12}$$

$$\lambda_2 = \frac{(v_0 \cdot v_0)(v_1 \cdot v_2) - (v_0 \cdot v_1)(v_0 \cdot v_2)}{(v_0 \cdot v_0)(v_1 \cdot v_1) - (v_0 \cdot v_1)(v_0 \cdot v_1)} \tag{13}$$

$$\lambda_3 = 1.0 - \lambda_1 - \lambda_2 \tag{14}$$

Since barycentric coordinates are a linear transformation of Cartesian coordinates, it follows that they change linearly along the sides and on the surface of the triangle. If a point is inside the triangle, all barycentric coordinates are inside the open interval (0.0 - 1.0). If the point lies on one of the sides of the triangle, at least one barycentric coordinate has the value 0.0, while the others are in the closed interval (0.0 - 1.0). Therefore, the point is inside the triangle if the condition is satisfied:

$$0.0 \le \lambda_i \le 1.0, \quad i = 1,3 \tag{15}$$

When it is determined which element of the old mesh the current node belongs to, values of the point coordinates in the local coordinate system should be calculated. For this, Newton's method of solving a system of two equations with two unknowns is used. When the values of the local nodal coordinates are found, the physical quantities for the given node can be calculated by simple linear interpolation:

$$^{n+1}v_i = N_K \, ^n v_i^K, \quad i = 1,2 \tag{16}$$

$$^{n+1}p_i = N_K \, ^n p_i^K, \quad i = 1,2 \tag{17}$$

where are:

N_K - interpolation functions for the value of previously determined coordinates

$^n p_i^K$, $^n v_i^K$ - nodal values of pressures and velocity components for the element of the old mesh within which the observed node of the new mesh is located,

$^{n+1}p_i$, $^{n+1}v_i$ - pressure values and velocity components in the current node of the new mesh.

The upper left indices n and $n+1$ correspond to the values of pressure and velocity at the end of the current and at the beginning of the next time step, respectively.

However, when the new and old finite element meshes are overlapped, nodes of the new mesh appear that are outside of all the elements of the old mesh. This happens near the solid-fluid boundary, in the zone where in the current step is solid, and in the next step is fluid (Figure 7).

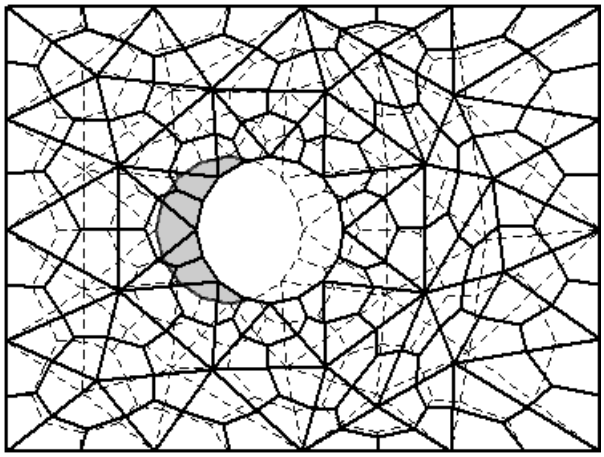

Figure 7: The zone (shaded in the figure) where there are nodes that cannot be interpolated

Interpolation of velocities and pressures for nodes in this area can be performed by building fictitious two-dimensional elements consisting of solid contour nodes and fluid contour nodes in the old finite element mesh, with known values of velocities (or pressures) for fluid nodes. One such element is shown in Figure 8.

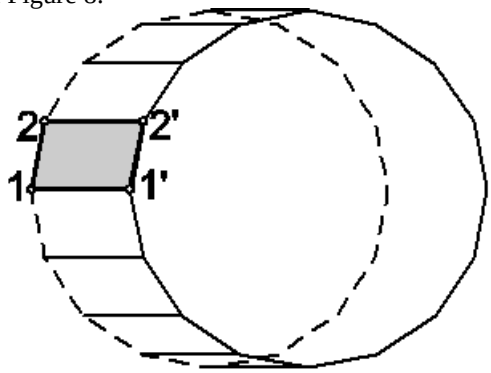

Figure 8: Fictitious 2D elements for interpolation of velocities and pressures

2.4 SSI Module: The interaction between two different solid domains

CSD solver can solve solid dynamics problems. But, for solving interaction problems, there is also a missing piece. Separated solid bodies are not aware of each other. In order to become aware, a mechanism of interaction should be implemented. This software solution uses the so-called elastic support methodology. It assumes finding the boundary nodes of a body that participate in mutual interaction with the boundary nodes of another body.

Figure 9 shows the model of interaction between two bodies. Each body is observed individually, and its position is compared with all other bodies. Let's take body A as an example. Any contour node of body A is examined if it falls within the interaction boundary of body B. If there is such a node, the algorithm adds an elastic support in the current node of body A perpendicular to the nearest segment of the contour of body B. This criterion is satisfied by nodes 1 and 2. Those nodes will be supported with the elastic supports with the direction perpendicular to the nearest segments of body B. Analogous to the previous one, it is checked whether any node of body B enters within the boundary of the interaction of body A. In this

case, node 3 satisfies the given criterion, and an elastic support perpendicular to the segment 1-2 of body A is placed in node 3.

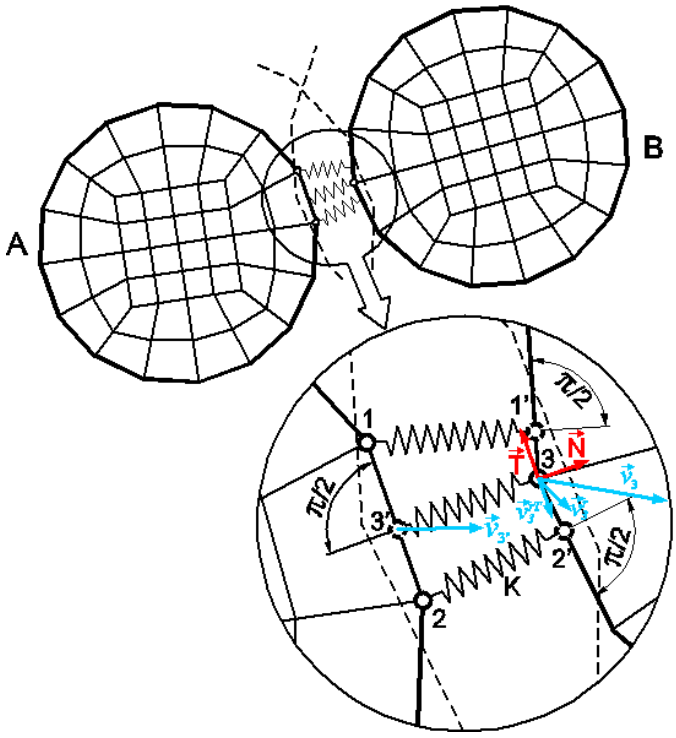

Figure 9: Solid-solid interaction model

The addition of elastic supports to the system is managed by an additional SSI module (Figure 10). The main components of SSI Module are: Node search engine - the component responsible for searching of interaction nodes; Elastic supports constructor - the component that builds elastic supports in interaction nodes; Equation assembler - the component that calculates local stiffness matrices and local forces and assembles them in coupled system of equations. The inputs in the SSI Module are geometrical positions of nodes and nodal displacements from the previous time step. The output of the SSI Module are element stiffness matrices and forces for all elastic supports constructed in current time step.

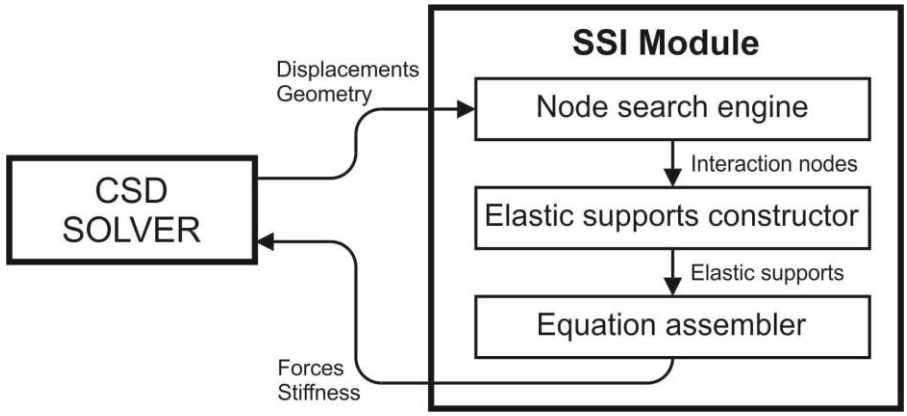

Figure 10: SSI Module

3. Results

3.1 Microfluidic chip

Malignant (tumor) cells have a higher stiffness than healthy cells (Lam et al. 2007; Suresh 2007; Scher et al. 2009). Since the dimensions of the cells are known, it is possible to design a chip with barriers and gaps such that the diameter of the cells is greater than the gap (like a filter). That allows healthy cells to deform and pass through the chip, while malignant cells, which have increased stiffness, cannot pass the gaps (Nagrath et al. 2007).
Figure 11.a shows a microscopic image of the microfluidic chip design. The chip is a miniature chamber interspersed with barriers and gaps where the tested blood flows through. Cell separation is performed under precisely controlled conditions of laminar flow.

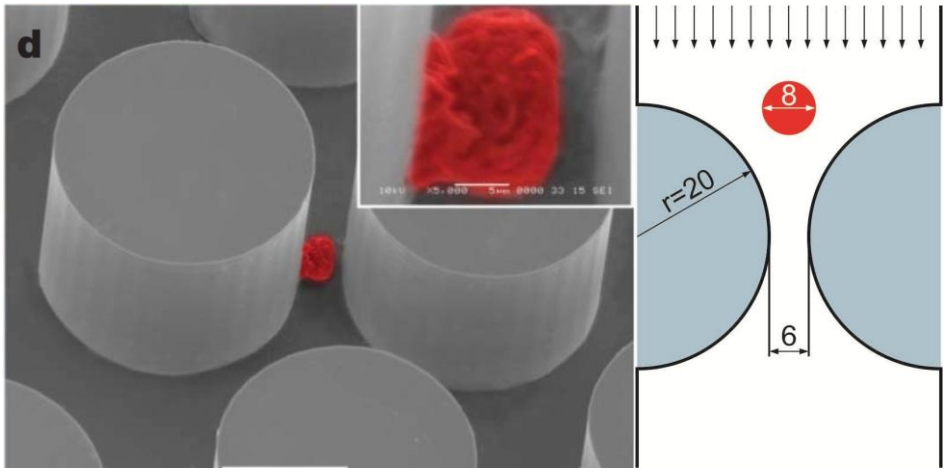

Figure 11: (a) Design of microfluidic chip (Nagrath et al. 2007), (b) Simplified computational model

Figure 11.b shows the geometry of a chip segment used to separate cells according to the stiffness value. The dimensions of the model are given in Figure 11.b. Material parameters for the solid are: modulus of elasticity $E = 200Pa$, Poisson's coefficient $\nu = 0.49$, density $\rho_s =$

$1.01 \cdot 10^3 kg/m^3$. The material characteristics of the fluid are the same as for human blood: fluid density $\rho_f = 1.0 \cdot 10^3 kg/m^3$, dynamic viscosity $\mu = 3.67 \cdot 10^{-3} Pas$. The inlet velocity of the fluid is $v = 100 \mu m/s$.

The cells move in parallel until the time $t = 2.0 \cdot 10^{-2} s$. From that moment they begin to enter the narrowing. From the time $t = 2.0 \cdot 10^{-2} s$ to $t = 2.4 \cdot 10^{-2} s$ cells enter the narrowing in parallel, and then one of the cells breaks in front of the other, due to the appearance of a slight asymmetry in the fluid velocities. Until the end of simulation ($t = 9.0 \cdot 10^{-2} s$) both cells pass through the narrowing.

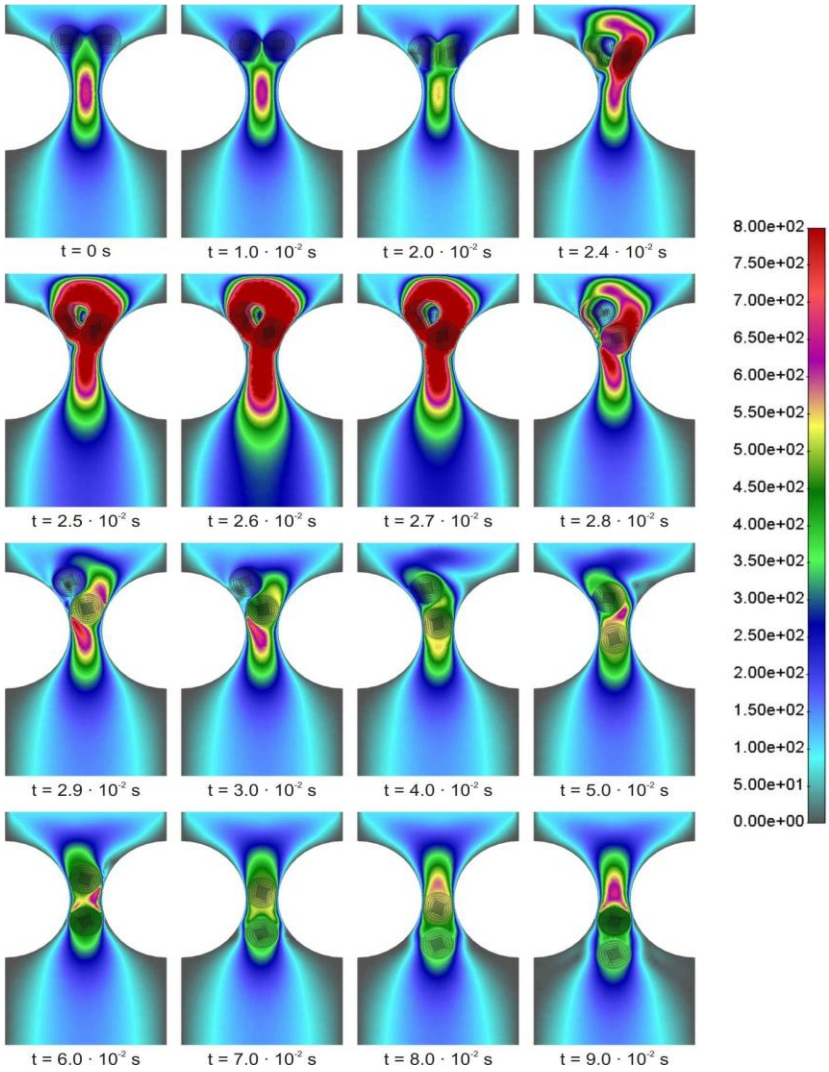

Figure 12: Passing two cells of equal stiffness through a microfluidic chip

In the second simulation, all parameters are the same, except Young's modulus for the cell placed right, which is increased 10 times (i.e. to simulate a cancer cell).

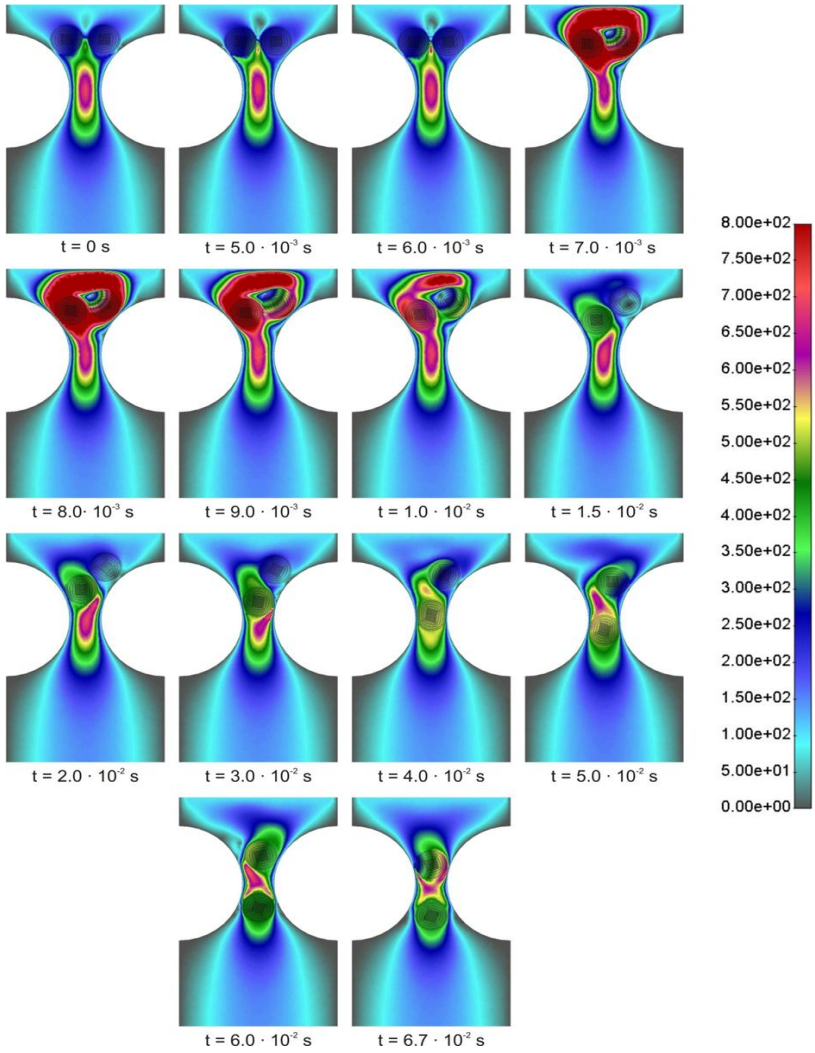

Figure 13: Passing two cells of different stiffness through a microfluidic chip (10 times increased Young's modulus for one cell)

By time $t = 6.7 \cdot 10^{-2} s$ the softer cell (placed left) passes the narrowing while the harder one remains stuck in the narrowing.

Discussion. The problem of solid motion in a fluid is very complex from the modeling point of view. That includes modeling the solid body dynamics, viscous fluid dynamics, interaction between solid and fluid, and interaction between two solids. All these processes take place inside a microfluidic chips.

As results show, it is possible to develop a software as a computational replica of the microfluidic chip, based on the experimental results, such that satisfactorily approximates real chip and its behavior.

Once the software is created, it can be used for a series of in-silico experiments, which can improve the design of the chip interior, without physically building it. This can significantly decrease the cost of chip development.

The software can give an insight in processes occurring within the chip itself, which cannot be physically observed. It is possible to see the way the cells are deformed, the velocity of the fluid flow between the cells, the pressures in the fluid before and behind the cell when it is in a chip's narrowing, etc.

Besides all the mentioned advantages brought by the computational model of the microfluidic chip, there are also certain limitations and barriers.

With today's hardware resources available to research centers, it is not possible to model and run a simulation for an arbitrary model size. The reasons are insufficient processor's power and insufficient amount of RAM memory. However, this can be overcome by using commercial supercomputing centers' resources or scientific centers whose supercomputing resources are available to the scientific community.

In order to develop appropriate computational model, very expensive experimental equipment is needed to determine the material parameters required to make the model reliable. Therefore, this kind of computational model is usable only by laboratories or centers already engaged in the design of microfluidic chips.

In order to reduce the level of approximation, more detailed cell's shape modeling is required. The realistic geometry can be achieved by reconstruction cell geometry from micro-CT medical images. Also, material models that more closely approximate the behavior of certain parts of the cells (cell membrane, etc.) can be used. They are available from other software modules (Kojic et al. 2017).

3.2 Circulating tumor cell traversing capillary narrowing

We consider the motion of a cell within the flowing blood entering a capillary with a narrowing. The model geometry, representing an axisymmetric channel with a cell approaching a capillary constriction, is illustrated in Fig. 14. The inlet and capillary diameters are 30 μm and 7 μm, respectively. A pressure gradient P induces motion of the fluid and the cell from left to right. The inset highlights the interaction between the cell and the channel wall, where repulsive spring-like forces act on the cell within a 0.75 μm distance from the wall. The cell–wall interaction, as well as the cell's motion within the fluid, is modeled as described in Section 2. We have used Newton fluid for the blood, a viscoelastic model for the cell, and an elastic material for the wall. Details are given in Kojic N. et al. 2015. Figure 15 shows the fluid velocity field for three positions of the cell. Note that the deformation of the cell for the position c) is very large.

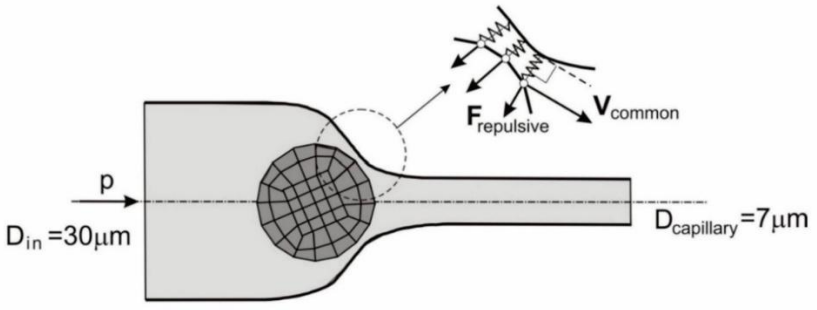

Figure 14: Model geometry of the axisymmetric channel inlet capillary diameters were 30μm and 7μm, respectively. The inset illustrates the interaction between the cell and the channel wall, where repulsive spring-like forces are applied when the cell is within 0.75 μm of the wall (according to Kojic N. et al. 2015).

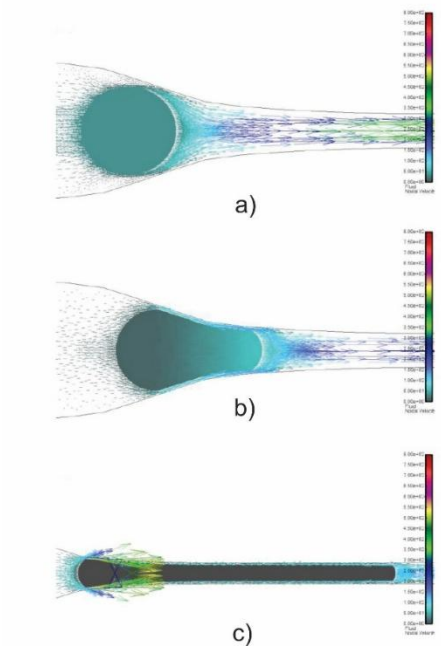

Figure 15: Fluid velocity field for three positions of the cell with the initial diameter of 18μm. a) Entering the capillary; b) Partially inside the capillary; c) Just inside the capillary (solid velocity omitted for clarity). Scalebars are the same for all panels. (according to Kojic N. et al. 2015).

A detailed analysis of the relationship between cell diameter, the pressure needed for the cell to pass to the capillary, and cell stiffness is given in Kojic N. et al. 2015. We here in Figure 16 show our results which also display the analytical relationship derived from computational results.

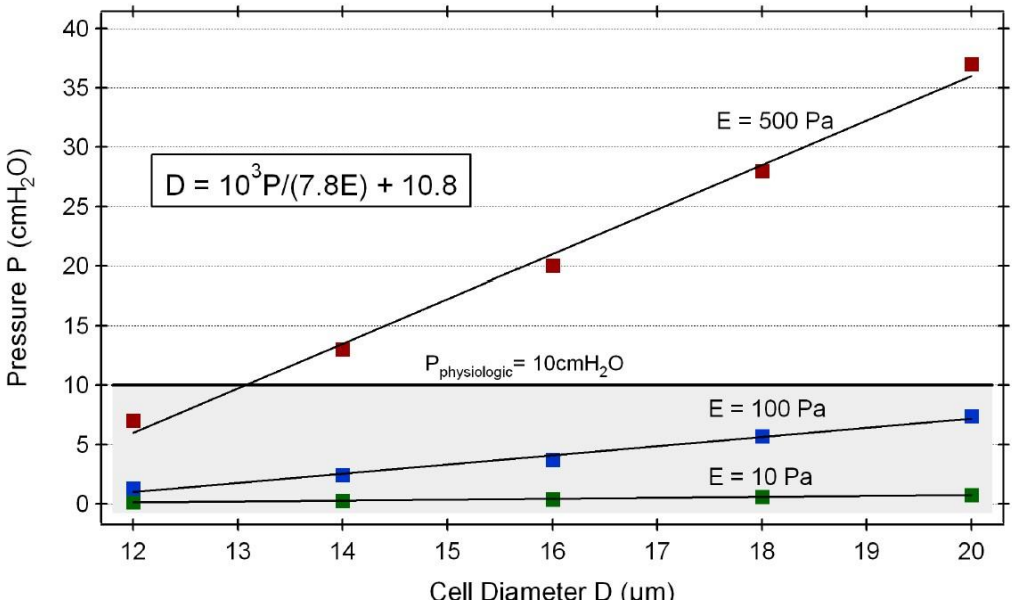

Figure 16: Fluid pressure required for CTC passage through a 7 µm capillary as a function of cell diameter and stiffness. Each point represents an individual simulation; points of the same color correspond to the same cell stiffness (green: 10 Pa, blue: 100 Pa, red: 500 Pa). Solid lines indicate linear fits for data points of identical stiffness. The shaded region below the typical physiological pressure line (P=10 cmH_2O) denotes conditions allowing capillary passage, with points within this region representing CTCs capable of traversing the capillary. The overall linear trend illustrates the derived relationship among fluid pressure, cell diameter, and cell stiffness (according to Kojic et al., 2015).

Conclusion

We presented our methodology for finite element modeling motion deformable bodies within the fluid. This methodology relies on the remeshing procedure which provides, at each time step, the coincidence between FE nodes at the common boundary between solid and fluid domains. This procedure demands significant computational efforts, but we found that it is advantageous regarding accuracy with respect to other methods, such as, for example, the immersed boundary method. This feature of our concept, built into our FE software PAK, is demonstrated in our numerous publications.

Two typical applications are selected which are based on our previous publications;both are of interest in biomedicine.

The first example, the microfluidic chip, is a device for blood testing for early detection of various types of malignant diseases. By detecting tumors at an early stage, the further growth and development of tumors as well as the occurrence of metastases can be largely prevented. Using microfluidic chips, it is possible from a very small blood sample to determine whether malignant cells exist in the blood providing almost non-invasive detection of early-stage malignant diseases. Microfluidic chip design can be significantly improved by using its

computational replica – a computer program that satisfactorily approximates the geometry of the chip and the processes occurring inside.

In the second example, which also is related to metastasis, we explored the parameter space, where a relationship between the capillary blood pressure gradient and the circulating tumor cells (CTCs) mechanical properties (size and stiffness) was determined for the CTC arrest in a capillary.

The presented methodology and the developed software provide capabilities in disease detection and progression and may be further used in biomedical research and ultimately in medical practice.

Acknowledgment

This research was supported by the Ministry of Education, Science and Technological Development of the Republic of Serbia through project ON174028: Multiscale Methods and Their Application in Nanomedicine. The authors acknowledge continuous support from the City of Kragujevac, Serbia, and the Serbian Academy of Sciences and Arts, Grant F-134.

References

Aceto N., Bardia A., Miyamoto David T., Donaldson Maria C., Wittner Ben S., Spencer Joel A., Yu M., Pely A., Engstrom A., Zhu H., Brannigan Brian W., Kapur R., Stott Shannon L., Shioda T., Ramaswamy S., Ting David T., Lin Charles P., Toner M., Haber Daniel A., Maheswaran S., Circulating Tumor Cell Clusters Are Oligoclonal Precursors of Breast Cancer Metastasis, Cell, 158, 1110-1122, 2014.

Amestoy P., Duff I., L'Excellent Y.I. and Koster J., A Fully Asynchronous Multifrontal Solver Using Distributed Dynamic Scheduling. SIAM J. Matrix Anal. Appl. Volume 23, 1999.

Balzer E.M., Konstantopoulos K., Intercellular adhesion: mechanisms for growth and metastasis of epithelial cancers, Wiley Interdiscip. Rev.-Syst. Biol, 4, 171-181, 2012.

Berne R.M., Koeppen B.M., Stanton B.A., Berne and Levy Physiology, Mosby/Elsevier, 2010.

Bradley C. J., The Algebra of Geometry: Cartesian, Areal and Projective Coordinates, Highperception, 2007.

Cho E.H., Wendel M., Luttgen M., Yoshioka C., Marrinucci D., Lazar D., Schram E., J. Nieva, L. Bazhenova, Morgan A., Ko A.H., Korn W.M., Kolatkar A., Bethel K., Kuhn P., Characterization of circulating tumor cell aggregates identified in patients with epithelial tumors, Phys. Biol., 9, 2012.

Fabienne D. Schwab, Manuel C. Scheidmann, Lauren L. Ozimski, André Kling, Lucas Armbrecht, Till Ryser, Ilona Krol, Karin Strittmatter, Bich Doan Nguyen-Sträuli, Francis Jacob, André Fedier, Viola Heinzelmann-Schwarz, Andreas Wicki, Petra S. Dittrich & Nicola Aceto, MyCTC chip: microfluidic-based drug screen with patient-derived tumour cells from liquid biopsies, Microsystems & Nanoengineering, Volume 8, 2022.

Isailovic V., Numerical modeling of motion of cells, micro- and nano- particles in blood vessels, PhD Thesis, Faculty of Information Technology, Metropolitan University, Belgrade, 2012.

Isailovic V., Kojic M., Milosevic M., Filipovic N., Kojic N., A Ziemys., Ferrari M., A computational study of trajectories of micro- and nano-particles with different shapes in flow through small channels, Journal of the Serbian Society for Computational Mechanics, Vol. 8 No. 2, pp.14-28 UDC: 532.517.2, 2014.

Ito, Y., Delaunay Triangulation. In: Engquist, B. (eds), Encyclopedia of Applied and Computational Mathematics. Springer, Berlin, Heidelberg, 2015.

Karabacak N.M., Spuhler P.S., Fachin F., Lim E.J., Pai V., Ozkumur E., Martel J.M., Kojic N., Smith K., Chen P., Yang J., Hwang H., Morgan B., Trautwein J., Barber T.A., Stott S.L., Maheswaran S., Kapur R., Haber D.A., Toner M., Microfluidic, marker-free isolation of circulating tumor cells from blood samples, Nature Protocols, 9, 694-710, 2014.

Kojic M., Filipovic N., Stojanovic B., Kojic N., "Computer Modeling in Bioengineering – Theoretical Background, Examples and Software". John Wiley and Sons, 978-0-470-06035-3, England, 2008.

Kojic M., Filipovic N., Zivkovic M., Slavkovic R., Grujovic N., PAK Finite Element Program, Faculty of Mech. Eng., University of Kragujevac, Serbia, 2017.

Kojic M., Milosevic M., Kojic N., Isailovic V., Petrovic D., Filipovic N., Ferrari M., Ziemys A., Transport phenomena: Computational models for convective and diffusive transport in capillaries and tissue, in: Suvranu De, Wonmuk Hwang, Ellen Kuhl, Eds., Multiscale Modeling in Biomechanics and Mechanobiology, Springer, Chapter 7, 131-156, 2015.

Kojić N., Milošević M., Petrović D., Isailović V., Sarioglu A. Fatih, Haber Daniel A., Kojić M., Toner M., A computational study of circulating large tumor cells traversing microvessels, Computers in Biology and Medicine, 63, 187–195, 2015.

Lam W.A., Rosenbluth M.J., Fletcher D.A., Chemotherapy exposure increases leukemia cell stiffness, Blood, Volume 109, 2007.

Lam W.A., Fletcher D.A., Cellular Mechanics of Acute Leukemia and Chemotherapy, in: A. Gefen (Ed.) Cellular and Biomolecular Mechancis and Mechanobiology, Springer, New York, pp. 523-558, 2011.

Lianidou E.S., Markou A., Circulating Tumor Cells in Breast Cancer: Detection Systems, Molecular Characterization, and Future Challenges, Clin. Chem., 57, 1242-1255, 2011.

Lichtman M.A., Rheology of leukocytes, leukocyte suspensions, and blood in leukemia - possible relationship to clinical manifestations, J. Clin. Invest., 52, 350-358, 1973.

Maheswaran S., Haber D.A., Circulating tumor cells: a window into cancer biology and metastasis, Curr. Opin. Genet. Dev., 20, 96-99, 2010.

Maton A., Human Biology and Health, Pearson Prentice Hall, 1993.

Milasinovic D., Vukicevic A., Filipovic, N., dfemtoolz: An open-source C++ framework for efficient imposition of material and boundary conditions in finite element biomedical simulations, Computer Physics Communications, Volume 249, 2020.

Nagrath S., Sequist Lecia V., Maheswaran S., Bell Daphne W., Irimia D., Ulkus L., Smith Matthew R., Kwak Eunice L., Digumarthy S., Muzikansky A., Ryan P., Balis Ulysses J., Tompkins Ronald G., Haber Daniel A., Toner M., Isolation of rare circulating tumour cells in cancer patients by microchip technology, Nature Letters, Volume 450, 2007.

Ozkumur E., Shah A.M., Ciciliano J.C., Emmink B.L., Miyamoto D.T., Brachtel E., Yu M., Chen P.I., Morgan B., Trautwein J., Kimura A., Sengupta S., Stott S.L., Karabacak N.M., Barber T.A., Walsh J.R., Smith K., Spuhler P.S., Sullivan J.P., Lee R.J., Ting D.T., Luo X., Shaw A.T., Bardia A., Sequist L.V., Louis D.N., Maheswaran S., Kapur R., Haber D.A., Toner M., Inertial Focusing for Tumor Antigen-Dependent and -Independent Sorting of Rare Circulating Tumor Cells, Sci. Transl. Med., 5, 2013.

Pantel K., Brakenhoff R.H., Brandt B., Detection, clinical relevance and specific biological properties of disseminating tumour cells, Nat. Rev. Cancer, 8, 329-340, 2008.

Rosenbluth M.J., Lam W.A., Fletcher D.A., Force microscopy of nonadherent cells: A comparison of leukemia cell deformability, Biophys. J., 90, 2994-3003, 2006.

Shewchuk J. R., Triangle: A Two-Dimensional Quality Mesh Generator and Delaunay Triangulator, University of California at Berkeley, Berkeley, California 94720-1776

Shibue T., Weinberg R.A., Metastatic colonization: Settlement, adaptation and propagation of tumor cells in a foreign tissue environment, Semin. Cancer Biol., 21, 99-106, 2011.

Si-Jie Hao, Yuan Wan, Yi-Qiu Xia, Xin Zou, Si-Yang Zheng, Size-based separation methods of circulating tumor cells, Advanced Drug Delivery Reviews, Volume 125, 2018.

Scher H. I., Xiaoyu J., de Bono Johann S., Fleisher M., Pienta Kenneth J., Raghavan D., Heller G., Circulating tumour cells as prognostic markers in progressive, castration-resistant prostate cancer: a reanalysis of IMMC38 trial data, The Lancet Oncology, Volume 10, Issue 3, 2009.

Stott S.L., Hsu C.H., Tsukrov D.I., Yu M., Miyamoto D.T., Waltman B.A., Rothenberg S.M., Shah A.M., Smas M.E., Korir G.K., Floyd F.P., Gilman A.J., Lord J.B., Winokur D., Springer S., Irimia D., Nagrath S., Sequist L.V., Lee R.J., Isselbacher K.J., Maheswaran S., Haber D.A., Toner M., Isolation of circulating tumor cells using a microvortex generating herringbone-chip, Proc. Natl. Acad. Sci. U. S. A., 107, 18392-18397, 2010.

Stott S.L., Lee R.J., Nagrath S., Yu M., Miyamoto D.T., Ulkus L., Inserra E.J., Ulman M., Springer S., Nakamura Z., Moore A.L., Tsukrov D.I., Kempner M.E., Dahl D.M., Wu C.L., Iafrate A.J., Smith M.R., Tompkins R.G., Sequist L.V., Toner M., Haber D.A., Maheswaran S., Isolation and Characterization of Circulating Tumor Cells from Patients with Localized and Metastatic Prostate Cancer, Sci. Transl. Med., 2, 2010.

Suresh S., Nanomedicine: Elastic clues in cancer detection, Nature Nanotechnology Volume 2, 2007.

Weinberg R., The Biology of Cancer, Second Edition, Garland Science. 2013.

Yu M., Bardia A., Wittner B., Stott S.L., Smas M.E., Ting D.T., Isakoff S.J., Ciciliano J.C., Wells M.N., Shah A.M., Concannon K.F., Donaldson M.C., Sequist L.V., Brachtel E., Sgroi D., Baselga J., Ramaswamy S., Toner M., Haber D.A., Maheswaran S., Circulating Breast Tumor Cells Exhibit Dynamic Changes in Epithelial and Mesenchymal Composition, Science, 339, 580-584, 2013.

Zhang Z., Xu J., Hong B., Chen X., The effects of 3D channel geometry on CTC passing pressure - towards deformability-based cancer cell separation, Lab on a Chip, 14, 2576-2584, 2014.